

New Features of Parenago's Discontinuity from Gaia DR1 Data

V. V. Vityazev^{*}, A. V. Popov^{**}, A. S. Tsvetkov^{***},
S. D. Petrov^{****}, D. A. Trofimov^{*****}, and V. I. Kiyayev^{*****}

St. Petersburg State University, Bibliotechnaya pl. 2, St. Petersburg, 198504 Russia

Received April 1, 2018

Abstract—The velocity field of main-sequence stars and red giants from the TGAS catalogue with heliocentric distances up to 1.5 kpc has been analyzed for various spectral types. To estimate the influence of a low accuracy of stellar parallax measurements on the results of a kinematic analysis of distant stars, first we have studied in detail how the kinematic parameters derived with $1/\pi$ distances are shifted when these distances are replaced by three other versions of distances from Astraatmadja et al. (2016b). We have obtained detailed tables in which the ranges of these shifts in the Ogorodnikov–Milne and Bottlinger model parameters are shown for the stars of each spectral type. We have the smallest shifts in the case of determining the Oort coefficients A and B , for which there are 10% shifts only for main-sequence stars of spectral type B. In the remaining cases, these shifts are 0–3%. For the remaining parameters the shifts do not exceed 30%. Thus, we have shown that using the $1/\pi$ distance scale in estimating the Ogorodnikov–Milne and Bottlinger model parameters (except for the parameter Ω_0'') yields reliable results even when using parallaxes with large relative errors (up to 60%). To study Parenago's discontinuity, we have investigated the dependence of the Ogorodnikov–Milne and Bottlinger model parameters on color for 1 260 071 main-sequence stars and 534 387 red giants. As far as we know, such a data set is used for the first time to investigate Parenago's discontinuity. The main result is the detection of maximum points at $B - V = 0.75$ after which the solar velocity component V and the Oort coefficient B decrease when moving from blue stars to red ones. This fact is a new feature of Parenago's discontinuity, because the component V does not change in the classical case at $B - V > 0.6$. We have made an attempt to represent the well-known Parenago's discontinuity as a special case of the more complex effect of a gradual change in a number of kinematic parameters as the mean age and composition of the group of stars under study changes.

DOI: 10.1134/S1063773718100080

Keywords: *proper motions, Gaia DRI, TGAS, Galactic kinematics, Parenago's discontinuity.*

INTRODUCTION

The dependence of kinematic parameters on color was found by Parenago in 1939 (Parenago 1950) and was named Parenago's discontinuity. This is how the dependence of the solar velocity, apex coordinates, and velocity ellipsoid parameters on spectral type is commonly called. This discontinuity has been repeatedly described or mentioned by various authors. The discontinuity is most pronounced for the solar velocity component V . Dehnen and Binney (1998) described this discontinuity as follows: the component V slowly increases for stars of spectral types from B to F and is virtually constant when passing from spectral type

F to G and further for later spectral types (see Figs. 3 and 4 in Dehnen and Binney (1998)). Having analyzed a sample of 11 865 main-sequence stars from the Hipparcos catalogue, Dehnen and Binney (1998) showed that $B - V = 0.61$ is a “break” point (the point at which the positive gradient becomes zero), which corresponds to spectral type G1 (Mihalas and Binney 1981).

Having analyzed the kinematics of 29 197 main-sequence stars and 17 465 red giants, Dobritko and Vityazev (2003) confirmed the existence of this break at $B - V = 0.6$ – 0.7 . At the same time, Parenago's discontinuity was not detected for red giants. In addition, using a three-dimensional version of the Hertzsprung–Russell diagram ($B - V, M_V, r$), the authors clearly showed that the point $B - V = 0.5$ separates the stars into two groups. The stars with $B - V > 0.5$ are nearby stars mostly closer than 100 pc from the Sun, while the stars with $B - V < 0.5$ are stars farther than 100 pc. At the same time,

*E-mail: vityazev@list.ru

**E-mail: 9141866@gmail.com

***E-mail: a.s.tsvetkov@inbox.ru

****E-mail: petr0v@mail.ru

*****E-mail: dm.trofimov@gmail.com

*****E-mail: kiyayev@mail.ru

the red giants are mostly located in the range 100–300 pc. Thus, Parenago’s discontinuity manifests itself when passing from the stars closer than 100 pc from the Sun to more distant stars.

Analyzing the velocity field of F and G dwarfs, Bobylev and Bajkova (2007) showed that the solar motion component Y depends on the residual velocity dispersion and stellar age and that the kinematics of stars belonging to the thin and thick Galactic disks is significantly different. At the same time, the kinematic parameters for various Galactic disk components also show a dependence on age, but already without any pronounced jumps.

Hai-Jun Tian et al. (2015) also detected Parenago’s discontinuity while analyzing the radial velocities of 200 000 FGK stars from the LAMOST DR1 catalogue. While investigating the velocity–temperature relation, they detected a “jump” in V and ascertained that the jump occurs at around $T_{\text{eff}} = 6000$ (5790) K, which, according to Sekiguchi and Fukugita (2000), corresponds to $B - V = 0.61$ (0.62). This, in turn, agrees well with the results of Dehnen and Binney (1998). In addition, they found that the kinematics of different layers in the Galactic disk differs.

The goal of this paper is to investigate Parenago’s discontinuity based on the proper motions of stars from the TGAS DR1 catalogue. In contrast to the previous papers, in which only the solar motion parameters and velocity ellipsoid parameters in the immediate solar neighborhood (up to 100 pc) are considered, we also studied the color dependence of the Ogorodnikov–Milne and Bottlinger model parameters determined for distant stars (up to 1.5 kpc). To estimate how the stellar parallax errors can affect the determinations of kinematic parameters, we, following the ideology of our previous paper (Vityazev et al. 2018), performed a kinematic analysis of stars in various $B - V$ color ranges for four versions of heliocentric distances provided for TGAS stars in Astraatmadja et al. (2016a, 2016b).

OGORODNIKOV–MILNE EQUATIONS

In our paper we used the Ogorodnikov–Milne model (Ogorodnikov 1965; du Mont 1977) to perform kinematic studies of the stellar proper motions from the TGAS catalogue. In this model the stellar velocity field is represented by the linear expression

$$\mathbf{V} = \mathbf{V}_0 + \boldsymbol{\Omega} \times \mathbf{r} + \mathbf{M}^+ \mathbf{r}, \quad (1)$$

where \mathbf{V} is the stellar velocity, \mathbf{V}_0 is the influence of the translational solar motion, $\boldsymbol{\Omega}$ is the angular velocity of rigid-body rotation of the stellar system, and \mathbf{M}^+ is the symmetric deformation tensor of the velocity field.

The Ogorodnikov–Milne model contains 12 parameters:

U, V, W are the components of the translational velocity vector of the Sun \mathbf{V}_0 relative to the stars;

$\omega_1, \omega_2, \omega_3$ are the components of the rigid-body rotation vector $\boldsymbol{\Omega}$;

$M_{11}^+, M_{22}^+, M_{33}^+$ are the parameters of the tensor \mathbf{M}^+ describing the velocity field contraction–expansion along the principal Galactic axes;

$M_{12}^+, M_{13}^+, M_{23}^+$ are the parameters of the tensor \mathbf{M}^+ describing the velocity field deformation in the principal plane and two planes perpendicular to it.

It is well known that the Ogorodnikov–Milne model parameters allow a number of kinematic and physical characteristics of our Galaxy to be estimated. First of all, the Oort constants are defined via them. Assuming that the velocity field is axisymmetric or $V_R = 0$, where V_R is the stellar velocity component along the radius vector in the Galactic cylindrical coordinate system (Miyamoto et al. 1993), for the Oort constants A and B we have

$$A = M_{12}^+, \quad B = \omega_3. \quad (2)$$

In turn, the Oort constants C and K are defined as follows:

$$C = \frac{M_{11}^+ - M_{22}^+}{2}, \quad K = \frac{M_{11}^+ + M_{22}^+}{2} - M_{33}^+. \quad (3)$$

These constants are linear combinations of the gradients of stellar velocity field parameters. The constants A and C describe the azimuthal and radial deformations, respectively, the constant B describes the rigid-body rotation component of the stars relative to the Galactic coordinate system, and K describes the field divergence (Torra et al. 2000).

With this notation, the conditional equations defining the stellar proper motions in the Ogorodnikov–Milne model are

$$\begin{aligned} \mathcal{K}\mu_l \cos b &= U/r \sin l - V/r \cos l \\ &- \omega_1 \sin b \cos l - \omega_2 \sin b \sin l + B \cos b \\ &- M_{13}^+ \sin b \sin l + M_{23}^+ \sin b \cos l \\ &+ A \cos b \cos 2l - C \cos b \sin 2l, \end{aligned} \quad (4)$$

$$\begin{aligned} \mathcal{K}\mu_b &= U/r \cos l \sin b + V/r \sin l \sin b \\ &- W/r \cos b + \omega_1 \sin l - \omega_2 \cos l \\ &- \frac{1}{2} A \sin 2b \sin 2l + M_{13}^+ \cos 2b \cos l \\ &+ M_{23}^+ \cos 2b \sin l \\ &- \frac{1}{2} C \sin 2b \cos 2l - \frac{1}{2} K \sin 2b. \end{aligned} \quad (5)$$

Given the solar velocity components U, V , and W , we can determine the solar velocity V_\odot relative to the

centroid of the set of stars under consideration and the solar apex coordinates L_{\odot} and B_{\odot} :

$$V_{\odot} = \sqrt{U^2 + V^2 + W^2}, \quad (6)$$

$$L_{\odot} = \arctan \frac{V}{U}, \quad (7)$$

$$B_{\odot} = \arctan \frac{W}{\sqrt{U^2 + V^2}}. \quad (8)$$

The Oort constants A and B allow the Galactic rotation parameters in the solar neighborhood to be estimated. Indeed, denoting the Galactocentric distance of the Sun by R_S , for the linear velocity of the Sun relative to the Galactic center we have

$$V_S = R_S(A - B). \quad (9)$$

With this velocity the Galactic rotation period is

$$P = \frac{2\pi R_S}{V_S}. \quad (10)$$

Note that in our paper we adopt $R_S = 8.0 \pm 0.2$ kpc (Vallee 2017).

The slope of the Galactic rotation curve or the Galactic rotation velocity gradient along the radius vector is defined by the expression (Vityazev and Tsvetkov 2012)

$$\frac{\partial V_S}{\partial R} = -(A + B). \quad (11)$$

BOTTLINGER FORMULAS

In this paper, apart from the linear three-dimensional Ogorodnikov–Milne kinematic model, we used a kinematic model based on the Bottlinger formulas (Kulikovskii 1985). In contrast the former model, it is assumed in the latter that the centroids move in circular orbits around the Galaxy's symmetry axis, with the orbital planes being parallel to the Galactic midplane. In this case, the basic kinematic equations are

$$\begin{aligned} V_r &= -U \cos l \cos b - V \sin l \cos b \\ &- W \sin b + R_0(R - R_0) \sin l \cos b \Omega'_0 \\ &+ 0.5R_0(R - R_0)^2 \sin l \cos b \Omega''_0 + Kr \cos^2 b, \end{aligned} \quad (12)$$

$$\begin{aligned} \mathcal{K}\mu_l \cos b &= U/r \sin l - V/r \cos l \\ &+ \Omega_0 \cos b - \frac{(R - R_0)}{r} (R_0 \cos l - r \cos b) \Omega'_0 \\ &+ \frac{0.5(R - R_0)^2}{r} (R_0 \cos l - r \cos b) \Omega''_0, \end{aligned} \quad (13)$$

$$\begin{aligned} \mathcal{K}\mu_b &= U/r \cos l \sin b + V/r \sin l \sin b \\ &- W/r \cos b - \frac{R_0(R - R_0)}{r} \sin l \sin b \Omega'_0 \end{aligned} \quad (14)$$

$$- \frac{0.5R_0(R - R_0)^2}{r} \sin l \sin b \Omega''_0 - K \cos b \sin b.$$

In these formulas the angular velocity of Galactic rotation at distance R_0 is denoted by Ω_0 , while the first and second derivatives of the angular velocity as functions of the distance R from the star to the Galactic rotation axis are denoted by Ω'_0 and Ω''_0 :

$$R^2 = r^2 \cos^2 b - 2R_0r \cos b \cos l + R_0^2. \quad (15)$$

In what follows, for the Galactocentric distance of the Sun we take $R_0 = 8.0 \pm 0.4$ kpc.

The parameters in these equations are related to the Oort coefficients as follows:

$$A = -0.5R_0\Omega'_0, \quad (16)$$

$$B = -\Omega_0 - 0.5R_0\Omega'_0, \quad (17)$$

$$A - B = \Omega_0. \quad (18)$$

DATA

Measurements onboard the Gaia spacecraft give not the distances to stars, but their trigonometric parallaxes. In the absence of parallax measurement errors, the heliocentric distances are calculated from the formula ($r = 1/\pi$). In what follows, we will designate the scale of such distances as Rpi. However, because of the ever-present parallax measurement errors, calculating the distances becomes a difficult problem that requires using a priori assumptions about the distribution of stars in space, photometric and spectroscopic characteristics of stars, their proper motions, and so on. The various methods of calculating the Rpi distance corrections are described in the literature (Lutz and Kelker 1973; Smith and Eichhorn 1996; Arenou 1999; Bailer-Jones 2015; Astraatmadja et al. 2016a, 2016b). All authors agree that no correction is required if the relative parallax measurement error does not exceed 10–20%. For this reason, in the overwhelming majority of papers samples of stars with small relative parallax errors are used and the distances are not corrected (Bovy 2017; Torra et al. 2000). As a consequence, comparatively nearby stars (up to 300–500 pc) are used in a kinematic analysis.

The paper by Astraatmadja et al. (2016b), where three versions of distances (Exp1, Exp2, and MW) based on different methods of simulating the spatial distribution of stars were calculated for all TGAS stars (irrespective of the relative parallax measurement error), appeared almost simultaneously with the publication of Gaia Data Release 1. The Exp1 and Exp2 distances were obtained within the model of

Table 1. Characteristics of the samples of main-sequence stars

Spectral type	O	B	A	F	G	K	M
$B - V$	< -0.3	$-0.3 : 0.0$	$0.0 : 0.3$	$0.3 : 0.58$	$0.58 : 0.85$	$0.85; 1.42$	> 1.42
$B - V$ mean	-0.37	-0.06	0.19	0.46	0.68	0.96	1.49
N	91	9195	189590	601577	425150	33843	625
σ_{π}/π	0.88	0.39	0.36	0.20	0.14	0.06	0.01
Rpi, kpc	2.54	1.15	0.98	0.56	0.36	0.15	0.03
MW, kpc	1.48	0.88	0.84	0.53	0.36	0.15	0.03
Exp1, kpc	0.78	0.59	0.59	0.45	0.33	0.14	0.03
Exp2, kpc	1.92	1.12	1.11	0.64	0.40	0.15	0.03

an exponentially decreasing space density of stars with increasing distance. Two versions of this model, Exp1 and Exp2, correspond to two scale lengths: $L = 1350$ pc (for the final composition of the Gaia catalogue) and $L = 110$ pc (for the TGAS catalogue). The MW version of distances is based on simulations of the distribution of stars in the Galaxy (Astraatmadja et al. 2016a).

Note that Astraatmadja et al. (2016b) warn that their distance scales should be used only for individual stars and should not be used in determining the mean distances to cluster stars or to establish the correspondence between the model distances and TGAS data. In our paper we determine neither the mean distances nor the model ones, but use various versions of individual distances to solve a completely different problem—to determine the parameters of the stellar velocity field. So, our approach is consistent with the warnings of the authors of the mentioned paper.

We used samples of stars from the TGAS catalogue referred to $B - V$ color ranges corresponding to different spectral types (Mihalas and Binney 1981). The characteristics of the samples of main-sequence stars drawn from the Hertzsprung–Russell diagram (Vityazev et al. 2018) constructed in the Rpi distance scale are given in Table 1. Analysis of this table leads us to the following conclusions.

- The smallest samples correspond to spectral types O (91 stars) and M (625 stars). For this reason, we do not consider these samples below.
- The mean relative parallax measurement errors that do not exceed 0.21 were obtained for spectral types F, G, and K.

- The mean relative parallax measurement errors that exceed 0.21 were obtained for spectral types B and A.
- The mean distances for the F, G, and K samples have small differences, in contrast to the B and A samples.

The characteristics of the samples of red giants drawn from the Hertzsprung–Russell diagram constructed in the Rpi distance scale are given in Table 2. Analysis of this table shows the following features.

- The bulk of the red giants are contained in the G and K samples.
- The mean relative parallax measurement errors for all three samples exceed a critical value of 0.2.
- For spectral types G and K the mean relative parallax measurement errors are within the range 0.36–0.41, while for the M sample this quantity is 0.57.
- For this reason, the distance scales for G and K stars, while not differing greatly between themselves, differ noticeably from the mean distances of the M sample.

In our study we used the APASS photometry as more accurate one (Henden et al. 2015). Unfortunately, the accuracy of the APASS photometry is low for bright stars ($m < 10$). For such stars we used the Hipparcos photometry.

Table 2. Characteristics of the samples of red giants

Spectral type	G	K	M
$B - V$	0.65 : 1.03	1.03 : 1.57	>1.57
$B - V$ mean	0.94	1.24	1.77
N	115 534	350 025	68 828
σ_{π}/π	0.36	0.41	0.59
Rpi, kpc	1.00	1.12	1.32
MW, kpc	0.85	0.96	1.11
Exp1, kpc	0.65	0.69	0.69
Exp2, kpc	1.17	1.33	1.64

STABILITY OF THE KINEMATIC PARAMETERS WITH RESPECT TO THE CHANGE OF DISTANCE SCALES

We estimated the Ogorodnikov–Milne and Bottlinger model parameters for the four versions of heliocentric distances to stars listed in the previous section. The calculations were performed based on the samples of main-sequence stars and red giants (Tables 1 and 2). Naturally, we are interested in the question of how much the estimates of the model parameters obtained with the Rpi scale are shifted when passing to the Exp1, Exp2, and MW scales. Denote the upper and lower boundaries of the parameters derived in all distance scales by a and b and the value corresponding to the Rpi scale by x . Based on the obvious inequality $a \leq x \leq b$, let us calculate the left-sided and right-sided possible relative shifts of the parameter x : $\alpha = (x - a)/|x|$ and $\beta = (b - x)/|x|$. The parameters α and β may be considered as measures of stability of the kinematic parameters when one distance scale is replaced by another. For example, if the largest of α and β is at a 5% level, then the parameters will change little and they may be deemed stable at a level of five percent. Conversely, if the largest of α and β exceeds 50%, then the parameters will change quite dramatically, i.e., they may be deemed strongly dependent on the distance scale. Note also that the sum $\gamma = \alpha + \beta$ is equal to the ratio of the length of the segment $[b - a]$ to $|x|$ and, consequently, is also a measure of accuracy (stability) with respect to the changes of distance scales.

Let us use these concepts to analyze our results. First consider the Ogorodnikov–Milne model parameters by dividing them into three groups: (1) the “solar terms” U, V, W ; (2) the Oort coefficients

A, B, C, K ; (3) the deformations and rotations in perpendicular planes $M_{13}, M_{23}, \Omega_2, \Omega_1$.

It can be seen from Tables 3 and 4 that the parameters U, V , and W for the main-sequence stars of spectral types B and A are most dependent on the distance scale. Here their relative shifts in the Rpi scale can reach 16%. The same shifts for spectral types F, G, and K do not exceed 3%, suggesting a weak dependence of these parameters on the applied distance scale. This difference between the spectral types is quite understandable, because, according to the data of Table 1, the relative parallax measurement errors for spectral types F, G, and K do not exceed 0.2. As regards the red giants, here the shifts of the parameters U, V , and W are within the range from 6 to 35%, which also corresponds to the data of Table 2. It follows from this table that here the relative parallax measurement errors for spectral types F, G, and K exceed 0.2.

It can be seen from Tables 3 and 4 that the Oort coefficients A and B are most sensitive to the distance scales when they are determined from both main-sequence stars and red giants. Indeed, their shifts can reach 10% only for the main-sequence stars of spectral type B. In the remaining cases, these shifts are 0–3% for the main-sequence stars and 0–6% for the red giants.

The sample of main-sequence B-type stars, where the shift can reach 77.5%, and the K sample, where the result is insignificant altogether, turns out to be least favorable when determining the parameter C . For the red giants shifts up to 26% are observed for spectral type G. As regards the parameter K , its shifts reach 18 and 16% only for the main-sequence stars of spectral type G. For the remaining stars these shifts are considerably smaller.

The parameters M_{23} and Ω_1 are determined from the main-sequence stars and red giants with shifts up to 29%, while the parameters M_{13} and Ω_2 are determined with shifts up to 15%.

Let us now consider the Bottlinger model parameters. The shifts of the parameters U, V , and W were found from the main-sequence stars and red giants to be almost equal to those in the Ogorodnikov–Milne model.

The parameters Ω_0 and Ω'_0 are virtually independent of the distance scale (the shifts do not exceed 4.4%). In turn, in view of Eqs. (16) and (17), this gives a very reliable determination of the Oort constants A and B , which are virtually independent of the distance scale. In contrast, Ω''_0 shows huge shifts (more than 100%), suggesting that this quantity depends strongly on the distance scale. For this reason, estimating this quantity requires additional justifications for the choice of a particular distance scale.

Table 3. Kinematic parameters in the Rpi scale for the spectral types of the samples of main-sequence stars. The Ogorodnikov–Milne model

	B	A	F	G	K
U	11.9 ± 0.2	9.7 ± 0.1	8.9 ± 0.1	9.1 ± 0.1	8.6 ± 0.2
Interval	[10.9; 12.4]	[8.9; 10.1]	[8.7; 9.1]	[9.0; 9.2]	[8.6; 8.6]
$\alpha; \beta$	[8.5%; 4.3%]	[8.4%; 4.5%]	[2.2%; 2.3%]	[0.6%; 1.4%]	[0%; 0%]
V	13.7 ± 0.2	12.4 ± 0.1	16.0 ± 0.1	22.5 ± 0.1	20.7 ± 0.2
Interval	[12.9; 14.2]	[11.8; 12.8]	[15.7; 16.4]	[22.3; 22.8]	[20.7; 20.7]
$\alpha; \beta$	[5.8%; 3.9%]	[5.0%; 3.0%]	[2.3%; 2.4%]	[0.6%; 1.4%]	[0%; 0%]
W	7.4 ± 0.2	6.8 ± 0.1	7.0 ± 0.1	7.4 ± 0.1	7.4 ± 0.2
Interval	[6.6; 7.8]	[6.2; 7.1]	[6.8; 7.2]	[7.4; 7.5]	[7.4; 7.4]
$\alpha; \beta$	[10.6%; 16.0%]	[8.7%; 5.1%]	[3.1%; 3.1%]	[0%; 1.8%]	[0%; 0%]
A	12.1 ± 0.4	14.1 ± 0.1	16.3 ± 0.2	17.9 ± 0.3	22.1 ± 2.8
Interval	[11.9; 13.0]	[13.7; 14.1]	[16.1; 16.3]	[17.8; 18.0]	[22.0; 22.1]
$\alpha; \beta$	[1.8%; 7.1%]	[2.9%; 0%]	[1.1%; 0%]	[0.8%; 0.3%]	[0.4%; 0%]
B	-13.4 ± 0.3	-13.1 ± 0.1	-12.5 ± 0.1	-11.9 ± 0.2	-14.5 ± 2.2
Interval	[-13.8; -12.0]	[-13.2; -12.5]	[-12.6; -12.4]	[-12.0; -11.9]	[-14.5; -14.5]
$\alpha; \beta$	[2.7%; 10.1%]	[1.3%; 4.6%]	[1.0%; 1.3%]	[0.9%; 0%]	[0%; 0%]
C	-2.4 ± 0.4	-4.5 ± 0.1	-3.9 ± 0.2	-4.5 ± 0.3	—
Interval	[-2.9; -0.5]	[-4.9; -3.2]	[-4.1; -3.4]	[-4.5; -4.4]	—
$\alpha; \beta$	[23.0%; 77.5%]	[9.2%; 27.9%]	[5.7%; 11.1%]	[0%; 1.2%]	—
K	-3.7 ± 1.4	-4.6 ± 0.4	-3.3 ± 0.3	-1.7 ± 0.6	—
Interval	[-3.7; -3.4]	[-4.7; -4.3]	[-3.3; -3.2]	[-2.1; -1.5]	—
$\alpha; \beta$	[1.2%; 7.0%]	[1.5%; 5.7%]	[0%; 2.2%]	[17.8%; 16.3%]	—
M_{23}	-4.4 ± 0.7	—	1.0 ± 0.2	1.5 ± 0.3	—
Interval	[-4.8; -4.3]	—	[0.7; 1.1]	[1.4; 1.6]	—
$\alpha; \beta$	[8.6%; 3.7%]	—	[28.8%; 7.8%]	[7.5%; 3.3%]	—
M_{13}	-3.2 ± 0.7	-1.7 ± 0.2	-1.4 ± 0.2	-1.3 ± 0.3	—
Interval	[-3.5; -3.0]	[-2.0; -1.7]	[-1.5; -1.3]	[-1.4; -1.3]	—
$\alpha; \beta$	[8.6%; 3.7%]	[15.2%; 0%]	[10.1%; 2.0%]	[5.3%; 0%]	—
Ω_1	5.0 ± 0.7	2.0 ± 0.2	2.1 ± 0.1	1.5 ± 0.3	—
Interval	[4.9; 5.1]	[1.9; 2.1]	[2.1; 2.1]	[1.3; 1.7]	—
$\alpha; \beta$	[0.9%; 3.0%]	[6.7%; 2.6%]	[0%; 0%]	[11.1%; 12.0%]	—
Ω_2	-3.1 ± 0.7	-1.5 ± 0.2	$-1, 4 \pm 0.2$	-1.5 ± 0.3	—
Interval	[-3.6; -3.0]	[-1.7; -1.5]	[-1.5; -1.4]	[-1.6; -1.5]	—
$\alpha; \beta$	[15.0%; 3.7%]	[10.1%; 0%]	[6.1%; 0%]	[-4.9%; 0%]	—

The intervals of values in the Exp1, Exp2, MW, and Rpi scales. α and β are the left-sided and right-sided deviations of the parameter estimate in the Rpi scale relative to the interval boundaries. The dashes mark those cases where the parameters turned out to be insignificant according to the three sigma rule. The spectral types of the samples of main-sequence stars are specified in the first row.

Table 4. Kinematic parameters in the Rpi scale for the spectral types of the samples of red giants

	G	K	M
U	10.0 ± 0.1	8.4 ± 0.1	6.8 ± 0.1
Interval	[8.8; 10.6]	[6.9; 9.3]	[4.4; 8.8]
$\alpha; \beta$	[11.3%; 6.1%]	[18.3%; 10.7%]	[34.8%; 30.3%]
V	24.9 ± 0.1	23.8 ± 0.1	22.9 ± 0.1
Interval	[21.9; 26.5]	[19.9; 25.5]	[17.1; 26.0]
$\alpha; \beta$	[12.1%; 6.3%]	[16.0%; 7.4%]	[25.5%; 13.3%]
W	6.3 ± 0.1	6.6 ± 0.1	5.3 ± 0.1
Interval	[5.5; 7.6]	[5.2; 7.4]	[3.5; 6.6]
$\alpha; \beta$	[16.7%; 9.5%]	[20.9%; 12.1%]	[33.1%; 25.3%]
A	11.7 ± 0.2	13.2 ± 0.1	12.6 ± 0.2
Interval	[11.4; 11.8]	[13.0; 13.4]	[12.3; 12.6]
$\alpha; \beta$	[2.4%; 0.8%]	[1.9%; 1.4%]	[2.2%; 0.4%]
B	-14.2 ± 0.2	-13.1 ± 0.1	-13.5 ± 0.1
Interval	[-14.5; -14.0]	[-13.3; -12.6]	[-13.8; -12.7]
$\alpha; \beta$	[2.1%; 1.4%]	[2.1%; 3.9%]	[2.7%; 5.5%]
C	-2.3 ± 0.2	-3.1 ± 0.1	-2.5 ± 0.2
Interval	[-2.6; -1.7]	[-3.3; -2.4]	[-2.7; -2.2]
$\alpha; \beta$	[14.2%; 25.6%]	[5.4%; 21.7%]	[6.4%; 12.3%]
K	-2.7 ± 0.4	-2.8 ± 0.2	-5.4 ± 0.5
Interval	[-2.9; -2.5]	[-3.0; -2.7]	[-5.7; -4.8]
$\alpha; \beta$	[7.7%; 7.1%]	[4.6%; 4.0%]	[5.1%; 10.9%]
M_{23}	—	-9.8 ± 0.1	—
Interval	—	[-0.8; -0.6]	—
$\alpha; \beta$	—	[0%; 24.0%]	—
M_{13}	—	-1.2 ± 0.1	—
Interval	—	[-1.3; -1.1]	—
$\alpha; \beta$	—	[13.2%; 3.0%]	—
Ω_1	—	—	-2.7 ± 0.3
Interval	—	—	[-3.0; -2.4]
$\alpha; \beta$	—	—	[9.7%; 9.8%]
Ω_2	—	-1.0 ± 0.1	-0.9 ± 0.3
Interval	—	[-1.0; -0.9]	[-1.2; -0.7]
$\alpha; \beta$	—	[0%; 5.6%]	[32.0%; 23.0%]

The intervals of values in the Exp1, Exp2, MW, and Rpi scales. α and β are the left-sided and right-sided deviations of the parameter estimate in the Rpi scale relative to the interval boundaries. The dashes mark those cases where the parameters turned out to be insignificant according to the three sigma rule. The spectral types of the samples of red giants are specified in the first row.

Table 5. Kinematic parameters in the Rpi scale for the spectral types of the samples of main-sequence stars. The Bottlinger model

	B	A	F	G	K
U	11.8 ± 0.2	9.6 ± 0.1	8.9 ± 0.1	9.1 ± 0.1	8.6 ± 0.2
Interval	[10.8; 12.3]	[8.8; 10.0]	[8.7; 9.1]	[9.0; 9.2]	[8.6; 8.6]
$\alpha; \beta$	[9.0%; 4.4%]	[8.3%; 4.5%]	[2.2%; 2.3%]	[0.6%; 1.3%]	[0%; 0%]
V	13.3 ± 0.2	12.2 ± 0.1	16.1 ± 0.1	22.6 ± 0.1	20.3 ± 0.2
Interval	[13.3; 13.8]	[12.1; 12.5]	[16.1; 16.3]	[22.6; 22.7]	[20.3; 20.4]
$\alpha; \beta$	[0%; 3.5%]	[1.0%; 1.8%]	[0%; 1.5%]	[0%; 0.5%]	[0%; 0.2%]
W	7.5 ± 0.1	6.9 ± 0.1	7.1 ± 0.1	7.4 ± 0.1	7.4 ± 0.2
Interval	[6.7; 7.9]	[6.3; 7.3]	[6.9; 7.3]	[7.3; 7.5]	[7.4; 7.4]
$\alpha; \beta$	[10.6%; 5.5%]	[9.1%; 5.1%]	[3.1%; 3.1%]	[0.7%; 1.8%]	[0%; 0%]
Ω_0	25.1 ± 0.5	27.1 ± 0.1	28.5 ± 0.2	29.7 ± 0.4	36.2 ± 3.5
Interval	[24.4; 25.3]	[26.0; 27.4]	[28.1; 28.7]	[29.7; 29.7]	[36.1; 36.2]
$\alpha; \beta$	[2.8%; 0.6%]	[4.4%; 1.0%]	[1.3%; 0.6%]	[0%; 0%]	[0.3%; 0.1%]
Ω'_0	-3.2 ± 0.1	-3.6 ± 0.1	-4.1 ± 0.1	-4.4 ± 0.1	-5.4 ± 0.7
Interval	[-3.2; -3.1]	[-3.6; -3.5]	[-4.1; -4.0]	[-4.5; -4.4]	[-5.4; -5.4]
$\alpha; \beta$	[0%; 4.3%]	[0%; 2.5%]	[0.3%; 0.8%]	[0.6%; 1.0%]	[0%; 0%]
Ω''_0	0.5 ± 0.1	0.3 ± 0.1	1.6 ± 0.1	3.3 ± 0.3	—
Interval	[0.4; 3.3]	[0; 1.8]	[0.7; 4.8]	[0.9; 6.6]	—
$\alpha; \beta$	[30%; 517%]	[103%; 404%]	[57%; 204%]	[73%; 109%]	—
K	-4.5 ± 1.4	-4.3 ± 0.4	-3.5 ± 0.3	-2.3 ± 0.6	—
Interval	[-4.6; -4.0]	[-4.4; -4.2]	[-3.5; -3.5]	[-2.5; -2.0]	—
$\alpha; \beta$	[1.7%; 11.9%]	[1.1%; 3.4%]	[0%; 0%]	[11.8%; 11.3%]	—
A	12.8 ± 0.4	14.2 ± 0.1	16.0 ± 0.2	17.8 ± 0.3	21.8 ± 2.8
Interval	[12.3; 12.8]	[13.8; 14.2]	[16.1; 16.3]	[17.6; 17.9]	[21.7; 21.8]
$\alpha; \beta$	[4.3%; 0%]	[2.5%; 0%]	[0.8%; 0.3%]	[1.0%; 0.6%]	[0.4%; 0.1%]
B	-12.3 ± 0.6	-12.9 ± 0.2	-12.3 ± 0.2	-12.0 ± 0.5	-14.4 ± 4.5
Interval	[-12.6; -11.8]	[-13.3; -12.1]	[-12.5; -11.9]	[-12.1; -11.9]	[-14.4; -14.4]
$\alpha; \beta$	[1.9%; 3.9%]	[2.8%; 6.4%]	[1.8%; 3.4%]	[1.1%; 0.9%]	[0%; 0%]

The intervals of values in the Exp1, Exp2, MW, and Rpi scales. α and β are the left-sided and right-sided deviations of the parameter estimate in the Rpi scale relative to the interval boundaries.

To summarize, it can be said that using the Rpi distance scale in estimating the Ogorodnikov–Milne and Bottlinger model parameters yields absolutely implausible results only for the parameter Ω''_0 in the Bottlinger model. In all the remaining cases, passing to the Exp1, Exp2, and MW scales causes shifts in the range from 0 to 30%. We have the most favorable situation in the case of determining the Oort coeffi-

cients A and B , for which there are shifts up to 10% only for the main-sequence stars of spectral type B. In the remaining cases, these shifts are 0–6%. In any case, our Tables 3–6 not only give the intervals containing the values of the sought-for estimates, but also allow the kinematic parameters determined most reliably from various samples of stars on the Hertzsprung–Russell diagram to be identified.

Table 6. Kinematic parameters in the Rpi scale for the spectral types of the samples of red giants. The Bottlinger model

	G	K	M
U	10.0 ± 0.1	8.9 ± 0.1	7.1 ± 0.1
Interval	[8.9; 10.6]	[7.0; 7.5]	[4.7; 9.1]
$\alpha; \beta$	[11.3%; 6.1%]	[18.4%; 10.8%]	[34.1%; 28.5%]
V	24.1 ± 0.1	22.2 ± 0.1	20.8 ± 0.2
Interval	[23.0; 25.1]	[20.5; 23.2]	[18.0; 22.80]
$\alpha; \beta$	[4.3%; 4.3%]	[7.6%; 4.4%]	[13.5%; 9.6%]
W	6.9 ± 0.1	6.6 ± 0.1	5.5 ± 0.1
Interval	[5.7; 7.5]	[5.2; 7.3]	[3.7; 6.8]
$\alpha; \beta$	[23%; 14%]	[21.1%; 11.8%]	[32.8%; 24.3%]
Ω_0	25.9 ± 0.3	26.4 ± 0.1	25.9 ± 0.2
Interval	[25.4; 26.2]	[25.6; 26.7]	[24.8; 26.3]
$\alpha; \beta$	[2.2%; 1.2%]	[3.1%; 1.2%]	[4.2%; 1.8%]
Ω'_0	-2.9 ± 0.1	-3.3 ± 0.1	-3.2 ± 0.1
Interval	[-3.0; -2.9]	[-3.3; -3.3]	[-3.2; -3.0]
$\alpha; \beta$	[1.9%; 1.82%]	[0%; 0%]	[0%; 4.0%]
Ω''_0	-0.3 ± 0.1	-0.2 ± 0.1	–
Interval	[-0.8; 3.2]	[-0.6; 2.1]	–
$\alpha; \beta$	[164%; 1112%]	[225%; 1300%]	–
K	-2.6 ± 0.4	-2.6 ± 0.2	-4.1 ± 0.5
Interval	[-2.8; -2.4]	[-2.8; -2.4]	[-4.4; -3.6]
$\alpha; \beta$	[11.3%; 7.5%]	[5.8%; 10.2%]	[5.8%; 13.8%]
A	11.6 ± 0.2	13.4 ± 0.1	12.6 ± 0.2
Interval	[11.4; 11.9]	[13.1; 13.4]	[12.1; 12.8]
$\alpha; \beta$	[1.8%; 1.9%]	[2.2%; 0%]	[4.0%; 1.0%]
B	-14.3 ± 0.4	-13.1 ± 0.2	-13.3 ± 0.3
Interval	[-14.7; -13.5]	[-13.4; -12.4]	[-13.6; -12.7]
$\alpha; \beta$	[3.0%; 5.5%]	[2.9%; 5.3%]	[2.5%; 4.4%]

The intervals of values in the Exp1, Exp2, MW, and Rpi scales. α and β are the left-sided and right-sided deviations of the parameter estimate in the Rpi scale relative to the interval boundaries.

ANALYSIS OF THE DEPENDENCE OF THE KINEMATIC PARAMETERS ON COLOR

Based on optimistic predictions of the accuracy for the kinematic parameters derived in the Rpi distance scale, let us now study the dependence of these quantities on the $B - V$ color or, equivalently, on the spectral type of the stars in our samples. For this purpose, using the samples of stars in $B - V$ with a 0.1^m step, we constructed the graphs (Figs. 1–4) on which the kinematic parameters are shown as

a function of $B - V$ for all four distance scales. A good consistency of the systematic behavior of the curves for all four distance scales is seen from these figures. There is a noticeable difference for $B - V < 0.3$ (spectral types B and A), whereupon the curves converge for late spectral types. This fact is easily interpreted, because, according to the data of Table 1, the accuracy of parallax determinations for distant

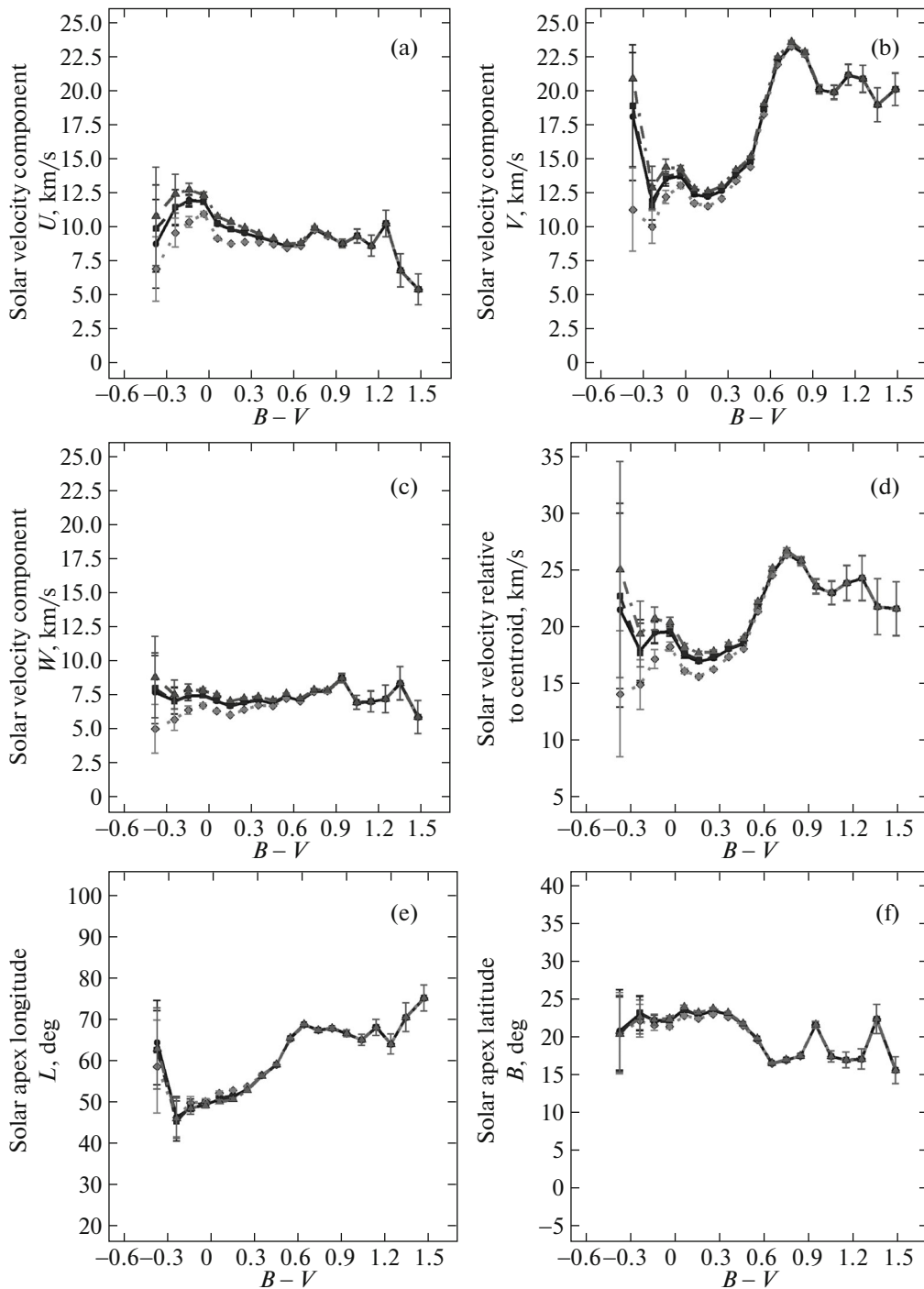


Fig. 1. Solar velocity components U (a), V (b), W (c), magnitude of the velocity V_0 (d), and solar apex coordinates (e, f) versus $B - V$ for the TGAS main-sequence stars in various versions of distances: the dots, dash-dotted line, dashed line, and solid line represent Exp1, Exp2, MW, and Rpi, respectively. The Ogorodnikov–Milne model.

stars increases when passing from distant stars to nearby ones.

A decrease in parameters U and W at $B - V > 1.3$ is seen from Figs. 1a and 1c, but the component V shows the most striking effect (Fig. 1b). Indeed, in the interval $[0.5; 0.74]$ the parameter V increases

linearly, then reaches a maximum of 23.3 km s^{-1} at $B - V = 0.74$, and subsequently begins to decrease at $B - V > 0.74$. Oscillations around the mean value of 20.2 km s^{-1} with an amplitude of 1 km s^{-1} are observed after $B - V > 1.2$. This fact is quite unexpected, because in the papers by Parenago (1950) and

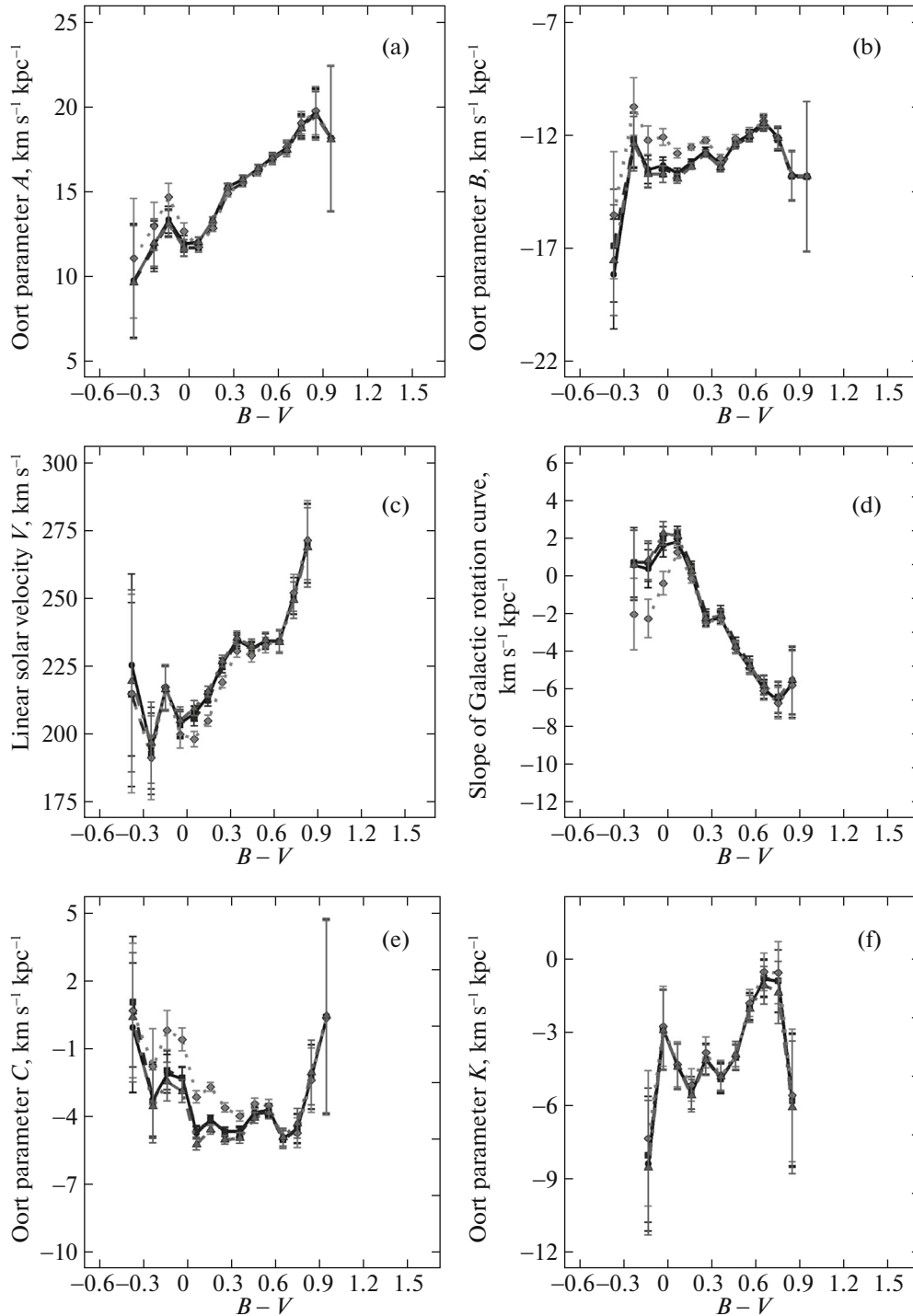


Fig. 2. Oort coefficients A , B , linear Galactic rotation velocity $V_S = R_S(A - B)$, and slope of the Galactic rotation curve versus $B - V$ for the TGAS main-sequence stars in various versions of distances: the dots, dash-dotted line, dashed line, and solid line represent Exp1, Exp2, MW, and Rpi, respectively. The Ogorodnikov–Milne model.

Dehnen and Binney (1998) we observe Parenago's plateau, where $V = 24 \text{ km s}^{-1}$, in the range $0.6 < B - V < 1.2$. Reflecting the above effects in the behavior of the components U , V , and W , the graph of the magnitude of the solar velocity in Fig. 1 shows

a similar picture at $B - V > 0.74$. The characteristic jumps in the gradients of the solar apex coordinates (Figs. 1e and 1f) are clearly seen at $B - V = 0.74$.

There is a monotonic increase up to $B - V = 0.9$ for the Oort coefficient A (Fig. 2a). Interestingly, a picture very similar to the behavior of the component

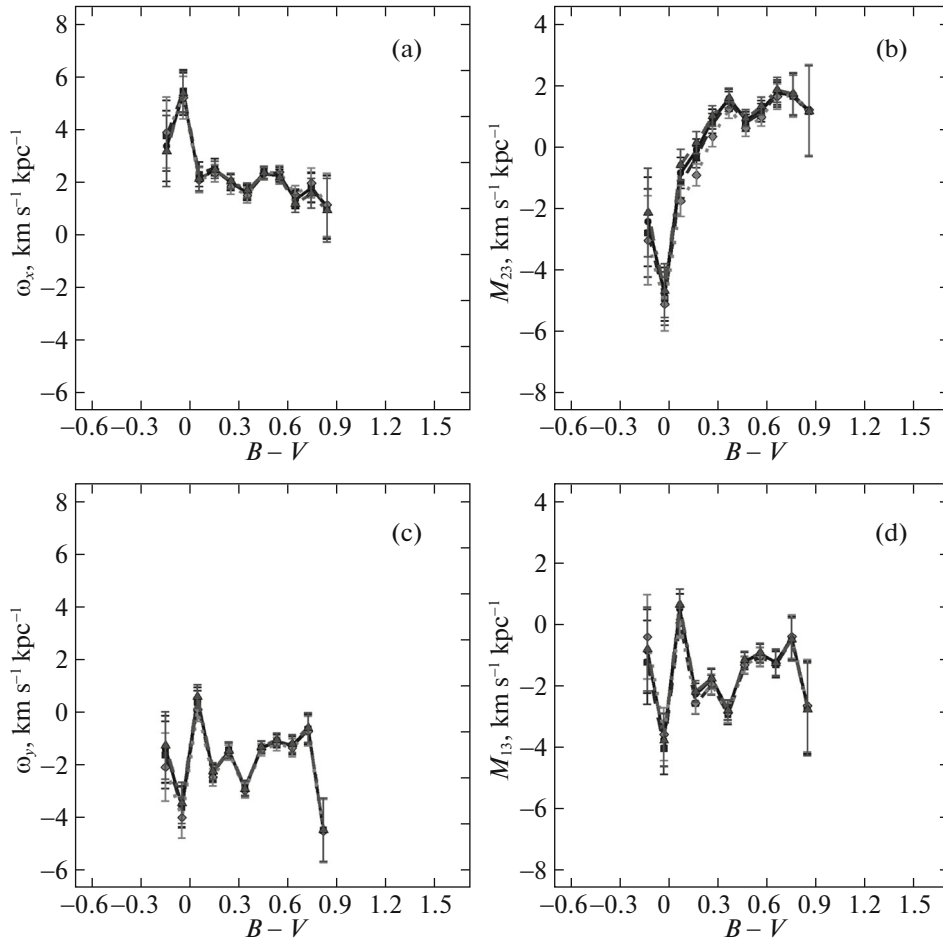


Fig. 3. Rigid-body rotation components ω_1 (a), ω_2 (c) and tensor parameters M_{23}^+ (b), M_{12}^+ (d) describing the velocity field contraction–expansion along the principal Galactic axes versus $B - V$ for the TGAS main-sequence stars in various versions of distances: the dots, dash–dotted line, dashed line, and solid line represent Exp1, Exp2, MW, and Rpi, respectively. The Ogorodnikov–Milne model.

V is observed for the Oort coefficient B (Fig. 2b). In the interval $[0.4; 0.75]$ we again have a positive gradient, then a maximum at $B - V = 0.75$, and then a decrease at $B - V > 0.75$. The linear Galactic rotation velocity (Fig. 2c) and the slope of the Galactic rotation curve (Fig. 2d) calculated via the Oort coefficients A and B show a strong dependence on $B - V$ with an abrupt change in the gradient at $B - V = 0.75$. The remaining Oort coefficients (C and K , Fig. 2) also show a dependence on $B - V$, with extrema near $B - V = 0.65$ – 0.75 being also observed here. Among the remaining Ogorodnikov–Milne model parameters Ω_x , M_{23}^+ , Ω_y , and M_{13}^+ (Fig. 3), only M_{23}^+ shows some semblance of Parenago’s discontinuity in its dependence on color.

Figure 4 shows the parameters peculiar to the Bottlinger model. Here we see that the parameter Ω_0 increases almost linearly with $B - V$ in the interval $[0.1; 0.4]$, the increases then ceases up to $B - V = 0.65$ and is resumed after $B - V = 0.65$. At $B - V =$

0.84 there is a maximum after which the parameter Ω_0 begins to decrease when moving toward red stars.

In turn, the parameter Ω'_0 behaves quite tranquilly, decreasing almost linearly with increasing $B - V$ and showing no features in the region of spectral types G and K.

The dependence of Ω''_0 on $B - V$ is very interesting. It has already been noted above that the estimates of this parameter differ greatly for different distance scales. Despite this fact, all four distance scales show the existence of a maximum at $B - V = 0.65$ and an abrupt drop in Ω''_0 when moving from the maximum point rightward.

Our sample of red giants refers to the range $0.9 < B - V < 2.0$, where Parenago’s plateau is located. For this reason, we cannot use the red giants to investigate the total Parenago’s discontinuity when passing from spectral type G to K. Nevertheless, some of the kinematic parameters of the red giants show a dependence on $B - V$ color even in the zone

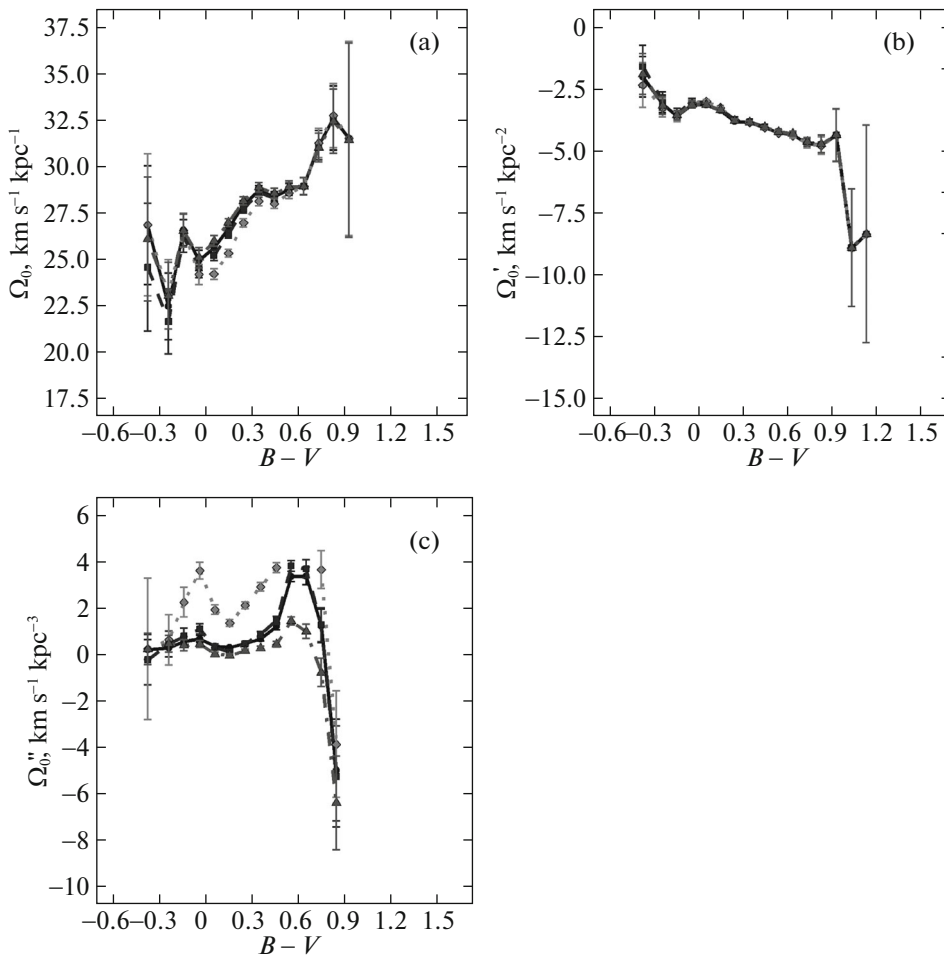


Fig. 4. Components Ω_0 (a), Ω'_0 (b), and Ω''_0 (c) versus $B - V$ for the TGAS main-sequence stars in various versions of distances: the dots, dash-dotted line, dashed line, and solid line represent Exp1, Exp2, MW, and Rpi, respectively. The Bottlinger model.

of Parenago's plateau. A study of these dependences is beyond the scope of this paper.

DISCUSSION

In our paper, having analyzed the data on 1 260 071 main-sequence stars, we see that there is a dependence on color not only for the solar velocity components relative to the centroids of the samples being analyzed, but also for other kinematic parameters. It is important to note that we observe no jumps in the kinematic parameters. Only the gradients of the change in parameters with color change abruptly. The extrema and jumps of the gradients occur at several characteristic values or intervals on the $B - V$ scale. For example, the maxima of the curves $V = V(B - V)$ and $B = B(B - V)$ take place at $B - V = 0.75$.

In turn, the intervals of positive gradients of the curves $V = V(B - V)$ and $B = B(B - V)$ are $0.5 < B - V < 0.75$ and $0.4 < B - V < 0.75$. Note also that there are similar results for the Bottlinger model

parameters. For example, zero gradient of the parameter Ω_0 occurs in the interval $0.4 < B - V < 0.65$, while the extremum of the dependence of Ω''_0 on color again falls at $B - V = 0.65$.

The main difference between our results and the classical ones is that $B - V = 0.61$ is no longer the point of discontinuity after which the parameter V takes a constant value (Parenago's plateau). In our case, $B - V = 0.75$ is the maximum point after which, when moving toward red dwarfs, the component V is on the decline and then shows oscillations around the mean $V = 20.2 \text{ km s}^{-1}$, which is smaller than Parenago's plateau, where $V = 24 \text{ km s}^{-1}$. This fact requires an explanation.

For this purpose, let us examine Fig 5 taken from Hai-Jun Tian et al. (2015) and supplemented by us with the data on the color (Sekiguchi and Fukugita 2000) and spectral type of stars (Mihalas and Binney 1981). The dependence of the stellar age on effective temperature, spectral type, and $B - V$ is shown here. We see the two features that we pointed

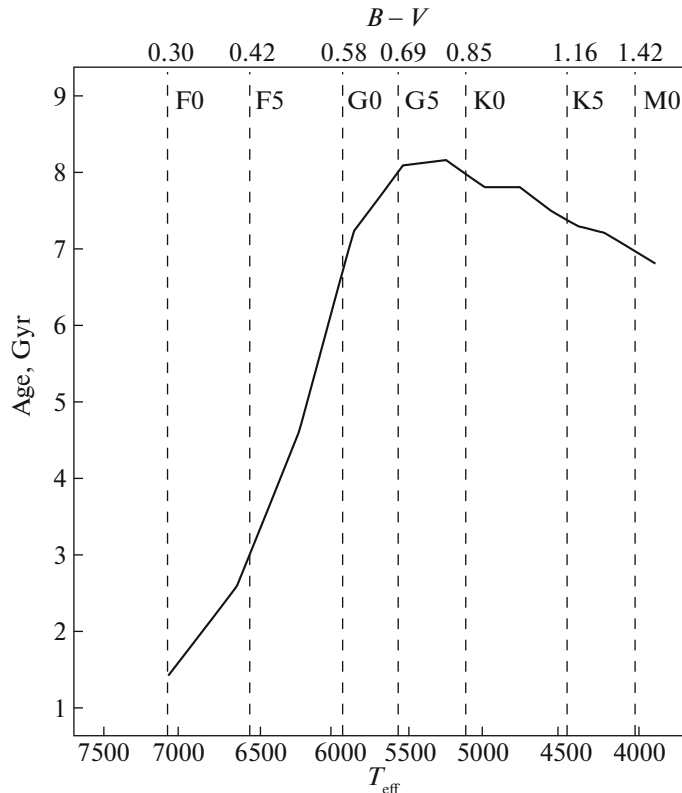


Fig. 5. Dependence of the stellar age on color, effective temperature, spectral type, and $B - V$.

out above in this figure as well: the characteristic point $B - V = 0.7$ and the interval $[0.4; 0.7]$ in which the stellar age increases rapidly from 3 to 8 Gyr followed by a slow decrease from 8 to 7 Gyr up to $B - V = 1.4$. This means that the cool stars had enough time to increase the velocity dispersion due to their scattering, which ultimately led to a decrease in the azimuthal solar velocity component V (Hai-Jun Tian et al. 2015). Interestingly, having drawn this conclusion from their analysis of the radial velocities of LAMOST DR1 stars, these authors found no decrease in the component V beyond $B - V = 0.6$. An increase in the stellar velocity dispersion must also lead to a decrease in the components U and W , which is observed in Figs. 1a and 1c beyond $B - V = 0.9$.

The fact that the errors in the model parameters increase sharply when passing from G to K stars, which can be explained by a larger velocity dispersion of K-type stars, is common to all parameters. A similar observation was pointed out in other papers (Dehnen and Binney 1998; Drobitko and Vityazev 2003; Bovy 2017).

Bobylev and Bajkova (2007) showed that the parameters U , V , and W derived from thin- and thick-disk stars differ significantly. Our results confirm these conclusions (Fig. 6). However, for both thin and thick disks we see the characteristic maxima in the dependence of the Oort coefficient B at $B -$

$V = 0.7$. Similarly, for the thin and thick disks the maxima of the curves $V = V(B - V)$ at $B - V = 0.7$ are retained. In both cases, we again observe the disappearance of Parenago’s plateau.

Note also that $B - V = 0.6$ in Dehnen and Binney (1998) and $B - V = 0.75$ in our paper play a special role. The first point corresponds to the transition from F to G and the classical Parenago’s discontinuity is observed at it. $B - V = 0.75$ corresponds to spectral type G5 and we have maxima of the parameters V and B at this point, these parameters then begin to decrease when moving toward red stars. The difference between these values corresponds to half of spectral type G. To all appearances, Parenago’s discontinuity is not “point-like,” but manifests itself differently for different subtypes of spectral type G. Based on the results of the studies listed above and our own results, we can say that, to all appearances, the manifestation of Parenago’s discontinuity as a “jump” in the component V is a special case of the dependence of kinematics on stellar color (age). This dependence generally manifests itself as jumps in the gradients of the change in parameters as functions of stellar color and as a decrease in the parameters V and B when passing from spectral type G to K.

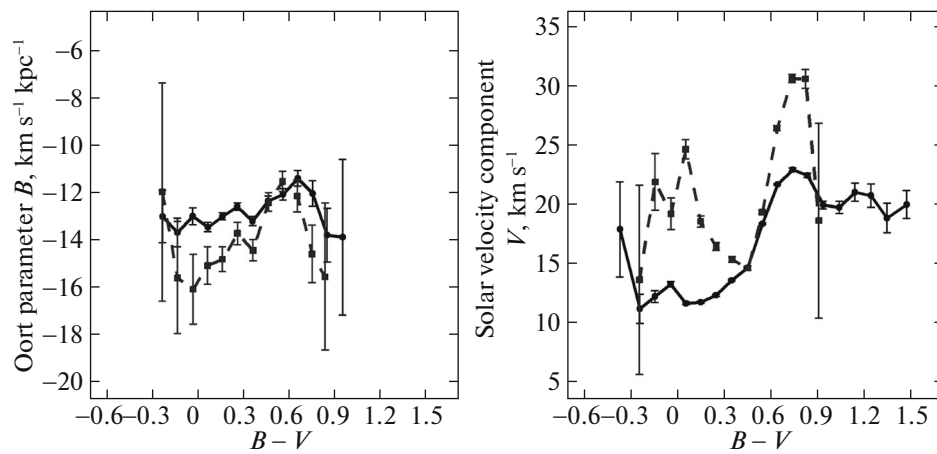


Fig. 6. Parameters B and V versus $B - V$ color. The Ogorodnikov–Milne model. The solid and dashed lines represent the thin disk $|z| < 0.25$ kpc and the thick disk $|z| > 0.25$ kpc, respectively.

CONCLUSIONS

Our study is devoted to the dependence of the Ogorodnikov–Milne and Bottlinger model parameters on color for main-sequence stars with heliocentric distances up to 1.5 kpc. To estimate the influence of a low accuracy of stellar parallax measurements on the results of a kinematic analysis of such distant stars, we first carried out a detailed study of how the kinematic parameters obtained with R_{pi} ($1/\pi$) distances were shifted when these distances were replaced by three other versions of distances provided for TGAS stars in Astraatmadja et al. (2016b).

We obtained the detailed Tables 3–6 in which our estimates of the shifts in the Ogorodnikov–Milne and Bottlinger model parameters calculated with the distance estimates from the formula $1/\pi$ relative to the distance estimates that take into account various models for the distribution of stars in the Galaxy are given for the stars of each spectral type. We established that changing the version of distances affects significantly the solar velocity components relative to the chosen centroid for the main-sequence stars of early spectral types B and A. For the main-sequence stars of spectral types F, G, and K the relative shifts of the solar terms do not exceed 3%. For the red giants the shifts of the parameters U , V , and W are within the range from 6 to 35%.

Among all the remaining kinematic parameters, the estimates of the Oort parameters A and B are least sensitive to the distance scales (shifts of 0–3% for most spectral types). For the remaining parameters the shift does not exceed 30%.

For the Bottlinger model the parameters Ω_0 and Ω'_0 are virtually independent of the distance scale (the shift does not exceed 4.4%). Thus, it can be asserted that using the $1/\pi$ distance scale in estimating the

Ogorodnikov–Milne and Bottlinger model parameters (except for the parameter Ω''_0) yields reliable results when using parallaxes with large relative errors (up to 60%).

In the second part of the paper we studied the dependence of the Ogorodnikov–Milne and Bottlinger model parameters on color for main-sequence stars. Note that we used the proper motions of more than a million stars. As far as we know, such a data set is used for the first time to investigate Parenago's discontinuity. The main result of this analysis is the detection of the maximum point $B - V = 0.75$ after which the solar velocity component V and the Oort coefficient B decrease when moving from blue stars to red ones. This fact is a new feature of Parenago's discontinuity, because the component V does not change in the classical case at $B - V > 0.6$. We made an attempt to represent the well-known Parenago's discontinuity as a special case of the more complex effect of a gradual change in a number of kinematic parameters as the mean age of the group of stars under study changes.

ACKNOWLEDGMENTS

We are grateful to the anonymous referee for useful remarks. This work was supported by St. Petersburg State University grant no. 6.37.343.2015.

REFERENCES

1. F. Arenou, ASP Conf. Ser. **167** (1999).
2. Astraatmadja, L. Tri, Bailer-Jones, and A. L. Coryn, *Astrophys. J.* **832**, 137 (2016a).
3. Astraatmadja, L. Tri, Bailer-Jones, and A. L. Coryn, *Astrophys. J.* **833**, 119 (2016b).
4. C. A. L. Bailerjones, *Publ. Astron. Soc. Pacif.* **127**, 994 (2015).

5. V. V. Bobylev and A. T. Bajkova, *Astron. Rep.* **51**, 372 (2007).
6. Jo Bovy, *Mon. Not. R. Astron. Soc. Lett.* **468**, L63 (2017).
7. W. Dehnen and J. J. Binney, *Mon. Not. R. Astron. Soc.* **298**, 387 (1998).
8. E. V. Drobit'ko, V. V. Vityazev, *Astrofizika* **46** (2) (2003).
9. A. A. Henden, S. Levine, D. Terrell, and D. L. Welch, *Am. Astron. Soc. Meet.* **225**, 336.16 (2015).
10. P. G. Kulikovskii, *Stellar Astronomy* (Nauka, Moscow, 1985)[in Russian].
11. L. Lindegren, U. Lammers, U. Bastian, et al., *Astron. Astrophys.* **595**, 323 (2016).
12. T. E. Lutz and D. H. Kelker, *Publ. Astron. Soc. Pacif.* **85**, 573 (1973).
13. D. Mihalas and J. Binney, *Galactic Astronomy. Structure and Kinematics*, 2nd ed. (ASP, San Francisco, 1981).
14. M. Miyamoto, M. Soma, and M. Yokoshima, *Astron. J.* **105**, 2138 (1993).
15. B. A. du Mont, *Astron. Astrophys.* **61**, 127 (1977).
16. K. F. Ogorodnikov, *Dynamics of Stellar Systems* (Fizmatgiz, Moscow, 1965)[in Russian].
17. P. P. Parenago, *Astron. Zh.* **27**, 150 (1950).
18. M. Sekiguchi and M. Fukugita, *Astron. J.* **120**, 1072 (2000).
19. H. Smith, Jr. and H. Eichhorn, *Mon. Not. R. Astron. Soc.* **281**, 211 (1996).
20. Hai-Jun Tian, Chao Liu, J. Carlin, Yong-Heng Zhao, Xue-Lei Chen, Yue Wu, G.-W. Li, Y.-H. Hou, and Y. Zhang, *Astrophys. J.* **809**, 145 (2015).
21. J. Torra, D. Fernandez, and F. Figueras, *Astron. Astrophys.* **359**, 82 (2000).
22. J. P. Vallee, *Astrophys. Space Sci.* **364**, 79 (2017).
23. V. V. Vityazev and A. S. Tsvetkov, *Astron. Lett.* **38**, 411 (2012).
24. V. V. Vityazev, A. V. Popov, A. S. Tsvetkov, S. D. Petrov, D. A. Trofimov, and V. I. Kiyayev, *Astron. Lett.* **44**, 236 (2018).

Translated by V. Astakhov